Hysteresis multicycles in nanomagnet arrays

J. M. Deutsch, Trieu Mai, and Onuttom Narayan
Department of Physics, University of California, Santa Cruz, California 95064, USA
(Received 14 September 2004; published 23 February 2005)

We predict two physical effects in arrays of single-domain nanomagnets by performing simulations using a realistic model Hamiltonian and physical parameters. First, we find hysteretic multicycles for such nanomagnets. The simulation uses continuous spin dynamics through the Landau-Lifshitz-Gilbert (LLG) equation. In some regions of parameter space, the probability of finding a multicycle is as high as ~ 0.6. We find that systems with larger and more anisotropic nanomagnets tend to display more multicycles. Our results also demonstrate the importance of disorder and frustration for multicycle behavior. Second, we show that there is a fundamental difference between the more realistic vector LLG equation and scalar models of hysteresis, such as Ising models. In the latter case spin and external field inversion symmetry is obeyed, but in the former it is destroyed by the dynamics, with important experimental implications.

DOI: 10.1103/PhysRevE.71.026120 PACS number(s): 05.50.+q, 82.40.Bj, 75.60.Ej, 61.46.+w

I. INTRODUCTION

Hysteresis in magnets [1,2] is a paradigm for all history dependent behavior in nature [3–5]. In addition, hysteresis is the cornerstone of the magnetic data storage industry, and of great technological importance [6]. Understanding the full possibilities of magnetic hysteresis is thus important for both fundamental insights and practical implications.

Recently, we have shown [7] that spin glasses can exhibit stable "multicycle" hysteresis loops, in that when the external magnetic field is cycled adiabatically (over a range that does not reach saturation), the magnetization returns to itself after $m>1$ cycles of the magnetic field. This behavior should be experimentally observable in spin glass nanoparticles at low temperature. Thus simple one-cycle hysteresis loops, although ubiquitous and generally assumed to be universal, are only part of a much richer phenomenon.

In our previous work [7], we used the standard Edwards-Anderson spin glass Hamiltonian [8], with Ising spins and nearest neighbor interactions in three dimensions. Zero temperature dynamics or Monte Carlo dynamics at low temperature were used. Starting from saturation, the magnetic field was lowered adiabatically, and then cycled repeatedly over a suitably chosen range. When the system reached steady state, the order of the multicycle (as defined in the previous paragraph) was measured. Whether a multicycle is present, and if so, its order, depended on the realization of randomness, varying from one system to another.

There were two weaknesses in the previous work. First, the systems considered were susceptible to thermal noise meaning that very low temperatures were needed to prevent fluctuations from destroying the periodicity. Second, the model considered was an Ising model. Although this has well defined equilibrium statistics, it is not clear that it adequately represents the dynamics.

In this paper, we overcome the problems of the previous paragraph by examining a different system as a candidate for multicycle hysteresis behavior: an array of magnetic nanoparticles. With current technology, it is standard to fabricate such magnetic arrays according to specification, and a wide variety has been studied experimentally [9] and these have important applications for magnetic storage technology, so called "patterned media" [10]. For our purposes, these systems offer many experimental advantages over the spin glass nanoparticles that we considered earlier. One can build "designer arrays" with optimized parameters that maximize multicycles and select them in a predictable manner. Spatially resolved measurements are possible, unlike for the spin glass case, making experimental observations of multicycles more practical. The relatively large size and shape of these also greatly reduce the effects of thermal noise (which is one important reason that they are useful in disk drive recording). Finally, the ability to address small regions of the array instead of only applying a uniform external magnetic field, and the sensitivity of multicycle phenomena to relatively small changes in system parameters, may open up the possibility of using these systems for computation.

Through numerical simulations, we demonstrate that multicycles can be seen in an array of pillars made of ferromagnetic material, coupled to each other through dipolar forces, arranged in square and triangular lattices. The external magnetic field is applied perpendicular to the lattice, i.e., parallel to the axes of the pillars; to be specific, we will refer to this as the vertical or z direction. The existence of multicycles is robust, persisting over a large range of system parameters.

We also examine the importance of frustration and disorder in achieving multicycles, a question that has been of great interest in spin glass research [8]. We find that when a square lattice is used instead of a triangular one, multicycles are not as likely to be seen. As discussed later in this paper, the magnetization in the pillars prefers to be approximately vertical, so that the dipolar coupling between the pillars is antiferromagnetic. For a square lattice, the dipolar forces between nearest neighbors are not frustrated, unlike the case for a triangular lattice. (There is still some frustration because of further neighbor interactions.) From this result, we conjecture that frustration plays an important role for the existence of multicycles. However, it has been shown [11] that systems with different coordination numbers have qualitatively different hysteresis loops regardless of the amount of frustration.

For the spin glass system considered earlier, disorder was explicitly present through the random bond strengths. For the nanoparticle array, although the bond strengths are not random (unless the spacings between the pillars are varied), there is crystalline anisotropy, arising from the fact that the magnetization prefers to align itself in a specific direction relative to the crystal axes. Because of the way in which the pillars are grown, the orientation of the crystal axes is different in each pillar, and random. Even if the crystalline anisotropy energy is small compared to the dipolar (and other) energies, we find that it is sufficient to cause multicycles in an otherwise regular triangular lattice. The order of the multicycle for a specific sample depends on the orientation of the crystalline axes in its pillars. Although in this paper we consider only the case of randomly oriented crystal axes, if the pillars could be grown with the orientations specified, it would be possible to make arrays whose hysteresis loops are multicycles of desired order.

Regardless of the source, it is desirable to have *some* inhomogeneity in the model to see multicycles. Without this, as the external magnetic field is reduced from saturation, the sequence in which the magnetic moments of the pillars changes depends strongly on thermal noise, and repeatable multicycles are not obtained for any given sample.

The model used for the dynamics in our numerical simulations is discussed in detail in the next section; the magnetic moment of each pillar is treated as a single "Heisenberg spin," i.e., with its orientation as a continuous variable, with continuous time dynamics. This is in contrast to the earlier spin glass work, with Ising spins and discrete (event driven) dynamics. Even though the dynamics are continuous, as discussed in the next section there is a shape anisotropy energy for tall pillars that causes the magnetization to be nearly vertical and to jump from up to down (or vice versa) as the external field is changed. This jump can trigger instabilities in other pillars, forming an avalanche. We believe that in order for multicycles to be seen, it is essential for the interaction between pillars to be sufficiently strong to cause avalanches; in the extreme case, when the pillars are independent, it is clear that a one-cycle hysteresis loop would be seen. However, avalanches are not sufficient to produce disorder: for disordered nearest neighbor Ising ferromagnets, the phenomenon of return point memory (RPM) [12,13] can be proved, precluding multicycles. This leads us to speculate that frustration is needed.

This is the first paper, as far as we are aware, that studies adiabatic hysteresis loops in magnetic systems using the more fundamental Landau-Lifshitz-Gilbert (LLG) equations rather than simplified relaxational dynamics. Experience from critical phenomena might lead one to believe that the difference between this approach and previous work would be trivial. However there is an important physical difference that we believe has been overlooked. LLG dynamics destroy symmetry under global spin flip, even though the Hamiltonian is symmetric under this operation. This mechanism for the asymmetry is impossible for scalar models such as Ising models. This result, which will be discussed further in the next section of this paper, has significant experimental implications [14].

In the next section of this paper, the dynamical equation used in the numerical simulations is introduced, and various terms in the model Hamiltonian are calculated. Details of the numerics are given in Sec. III, and the results thereof are presented in Sec. IV.

II. CLASSICAL SPIN DYNAMICS AND THE MODEL HAMILTONIAN

Microscopically, the evolution of classical spins is described by the Landau-Lifshitz-Gilbert equation of motion [15]. The LLG equation is the simplest equation describing micromagnetic dynamics which contains a reactive term and a dissipative term:

$$\frac{d\mathbf{s}}{dt} = -\gamma_1 \mathbf{s} \times \mathbf{B} - \gamma_2 \mathbf{s} \times (\mathbf{s} \times \mathbf{B}), \tag{1}$$

where $\mathbf{s}$ is a microscopic spin, $\mathbf{B}$ is the local effective field, γ_1 is a precession coefficient, and γ_2 is a damping coefficient. The effective field is $\mathbf{B} = -\partial \mathcal{H} / \partial \mathbf{s} + \boldsymbol{\zeta}$, where $\mathcal{H}$ is the Hamiltonian and $\boldsymbol{\zeta}$ represents the effect of thermal noise. Terms in the Hamiltonian will be discussed and computed later in this section.

The reactive term of the LLG equation describes the precession of the spin about its local field, with the angle between the two remaining constant. (The coefficient of the reactive term γ_1 will be set to unity throughout this paper unless otherwise noted.) The dissipative term aligns the spin with its local effective field. The cross products in the dissipative term ensure that only the tangential component of the field causes damping, since the length of $\mathbf{s}$ cannot change. The relaxation time is inversely related to the damping coefficient γ_2. Reasonable approximations for γ_2 are difficult to obtain, but it will be shown that the hysteresis multicycle phenomenon studied in this paper is present for a large range of γ_2.

With current technology, nanomagnetic pillars that are approximately 50 nm wide and 100 nm tall can be made of ferromagnetic materials such as nickel [9]. For such small pillars, it is found that the ferromagnetic coupling between the atoms dominates the antiferromagnetic dipolar interactions. Thus the entire pillar consists of a single magnetic domain. Using the lattice constant of nickel, each pillar holds approximately 10^7 atoms, allowing us to treat the pillar as a continuous magnetic medium. Edge effects such as splaying near the boundaries are neglected, and the pillar is treated as a saturated nanomagnet with uniform magnetization. Each single-domain nanomagnet can be viewed as a single degree of freedom: a magnetic moment of fixed magnitude, whose orientation represents the direction of the magnetization [16]. The time evolution of this magnetic moment has the *same* structure as the micromagnetic LLG equation: a reactive part $-\gamma_1 \mathbf{s} \times \mathbf{B}$, and a dissipative part $-\gamma_2 \mathbf{s} \times (\mathbf{s} \times \mathbf{B})$, although γ_2 is different from its microscopic value. (Henceforth $\mathbf{s}$ will denote a unit vector in the direction of the magnetic moment of a pillar, rather than an individual spin.) As before, the field $\mathbf{B}$ is given by $-\partial \mathcal{H} / \partial \mathbf{s}$; the large number of spins evolving in unison in each pillar allows the thermal noise $\boldsymbol{\zeta}$ to be neglected.

To complete the specification of the dynamics of the magnetic moments through Eq. (1), the Hamiltonian has to be

calculated in terms of the magnetic moment of each pillar. The various terms in the Hamiltonian are discussed in the following paragraphs.

First, the geometry of the pillars introduces a shape anisotropy term in the Hamiltonian:

$$\mathcal{H}_{SA} = -d_z \sum_i s_{z,i}^2, \tag{2}$$

where d_z is a constant to be calculated in the next paragraph and $s_{z,i}$ is the z component of the magnetic moment of the ith pillar. Shape anisotropy energy is present because of the dipolar interactions between the individual spins within a pillar. Qualitatively, if the magnetization of a tall skinny pillar is vertical, the spins are predominantly lined up "head to toe." This configuration has a lower energy than when the magnetization is horizontal, in which case the spins are predominantly side by side. For a short wide disk, the effect is clearly reversed.

For the case of tall pillars, the shape anisotropy reduces the magnetic moment to an almost Ising-like variable, that can (approximately) point only up or down. The dynamics of anisotropic and isotropic spins are qualitatively different, with avalanche phenomena more likely to occur in the former than the latter. As mentioned earlier, we believe that avalanches are necessary for hysteretic multicycles. Note that even when the shape anisotropy is large, we evolve each magnetic moment according to Eq. (1) rather than as an Ising variable, i.e., with an orientation that evolves continuously with time, although the shape anisotropy causes rapid transitions from up to down states.

Deriving the form of $\mathcal{H}_{SA}$ and the value of d_z requires solving a magnetostatic problem. The energy of the field due to the microscopic spins in a single pillar is $W = (1/2\mu_0)\int d^3x |\mathbf{B}(\mathbf{x})|^2$, where $\mathbf{B}(\mathbf{x})$ is the magnetic field at $\mathbf{x}$ due to the spins. Through Ampere's law and vector calculus manipulations, we can rewrite this in terms of the magnetization $\mathbf{M}(\mathbf{x})$. For uniform magnetization, the result can (up to an additive constant) be converted to a (quadruple) integral over two surfaces, similar to electrostatics, with the self-energy of the magnetic surface "charge" to be calculated. For cylindrical pillars, which we consider in the rest of this paper, if the magnetization has magnitude M_0 and makes an angle θ to the vertical, and R and h are the radius and height of the pillars, the final result is

$$W = \mu_0 M_0^2 R^3 F\left(\frac{h}{R}\right)\cos^2\theta \tag{3}$$

up to an additive constant independent of θ. Comparing with Eq. (2), we see that $d_z = -\mu_0 M_0^2 R^3 F(h/R)$, where $F(h/R)$ is a function of the aspect ratio that can be evaluated numerically. With M_0 equal to the saturation magnetization for nickel, 4.84×10^5 A/m [9], the values of d_z for different sized pillars are given in Table I. If the pillars are ellipsoidal instead of cylindrical, d_z can be obtained analytically instead of numerically [9,16].

A second form of anisotropy energy is caused by the crystal structure of Ni. As mentioned earlier, the crystal axes give a preferential direction to the magnetization, independent of the shape of the pillar. Nickel has a face-centered cubic structure which tends to align spins in the [111] direction. If $\alpha_{x,i}$, $\alpha_{y,i}$, and $\alpha_{z,i}$ are the direction cosines of the magnetization of the ith pillar to its (x,y,z) crystal axes, the crystal anisotropy energy can be expanded in powers of α. The first two terms are [9,16]

TABLE I. Calculated shape anisotropy coefficients d_z for pillars with radius $R=30$ nm and different aspect ratios h/R. The ratios between crystalline anisotropy coefficients and d_z are also given.

h/R	d_z (10^{-18} J)	$\lvert K_1/d_z\rvert$	$\lvert K_2/d_z\rvert$
0.5	−2.866	0.0740	0.0296
1	−2.689	0.1577	0.0631
2	0.769	1.102	0.441
3	5.754	0.2211	0.0885
4	11.30	0.1501	0.0600
5	17.11	0.1240	0.0496
10	47.41	0.0894	0.0358

$$\mathcal{H}_{CA} = \sum_i -\frac{K_1}{2}(\alpha_{x,i}^4 + \alpha_{y,i}^4 + \alpha_{z,i}^4) + K_2 \alpha_{x,i}^2 \alpha_{y,i}^2 \alpha_{z,i}^2, \tag{4}$$

where an additive constant has been dropped. The material parameters K_1 and K_2 can be obtained by multiplying the experimentally obtained energy densities by the volume of the pillars. Crystal anisotropy energy densities have approximate values of -5×10^3 and -2×10^3 J/m^3 for $K_1/\mathcal{V}$ and $K_2/\mathcal{V}$ respectively [9]. Athough the ratio of K_2/K_1 is $\sim$0.4, the first term dominates, since it has two fewer powers of α.

In addition to the shape and crystal anisotropies that affect each pillar by itself, there is dipolar coupling between pillars. Microscopically, this is similar to the shape anisotropy energy, except that it arises from interactions between spins on different pillars. The resultant interaction energy is of the form

$$\mathcal{H}_{dip} = \sum_{i,j\neq i} \mathbf{s}_i \cdot \mathsf{A}(\mathbf{r}_{ij}) \cdot \mathbf{s}_j. \tag{5}$$

$\mathsf{A}(\mathbf{r}_{ij})$ is a second-rank tensor that depends only on the separation of the pillars. The elements of $\mathsf{A}(\mathbf{r}_{ij})$ are determined by numerically solving integrals similar to the integrals for the shape anisotropy energy.

The last term in the Hamiltonian is due to the external magnetic field, which we take to be in the z direction. The form of this term is the conventional one, $\mathcal{H}_{ext} = -B_e \Sigma s_{z,i}$. Hysteresis occurs as B_e is varied adiabatically, with the system evolving according to the LLG equation.

In summary, the full Hamiltonian has four terms: shape anisotropy, crystalline anisotropy, external field, and dipole-dipole interaction. The first two are properties of the pillars individually, the external field term is the term that is adiabatically changed to observe hysteresis, and the dipole term is an interaction between pillars:

$$\mathcal{H} = \sum_i \left(- d_z s_{z,i}^2 - \frac{K_1}{2}(\alpha_{x,i}^4 + \alpha_{y,i}^4 + \alpha_{z,i}^4) + K_2 \alpha_{x,i}^2 \alpha_{y,i}^2 \alpha_{z,i}^2 - B_e s_{z,i} + \sum_{j \neq i} \mathbf{s}_i \cdot \mathsf{A}(\mathbf{r}_{ij}) \cdot \mathbf{s}_j \right). \quad (6)$$

In the numerics, the actual values of the coefficients in the Hamiltonian are inconsequential, and only the ratios of terms are relevant. Table I shows the results of the calculations described above for d_z, K_1, and K_2. Evidently, for the dimensions of the nanomagnetic pillars of interest, the shape anisotropy term is larger than the crystalline anisotropy. The dipolar coupling is also small compared to d_z for the lattice spacings of interest. In the simulations, all energies are normalized to d_z. Although d_z is dominant for pillars with aspect ratios of interest, the other terms must be included in the Hamiltonian because they affect the dynamics qualitatively. Without the dipole term, each pillar would be isolated. The crystalline anisotropy term introduces quenched randomness in the system, and determines the order in which the $\mathbf{s}_i$'s flip when the magnetic field is changed; its importance has been discussed toward the end of Sec. I. Thus the Hamiltonian of Eq. (6) has all the important terms that have to be kept.

As mentioned in Sec. I, although the Hamiltonian of Eq. (6) is invariant if all the $\mathbf{s}_i$'s are flipped (along with the external magnetic field), the dynamics of Eq. (1) are not. In Eq. (1), under spin and external field reversal, the left hand side and the dissipative term on the right hand side change sign, but the reactive term does not. Therefore the spin inversion symmetry, although relevant to equilibrium static properties, does not apply to the nonequilibrium dynamics appropriate for hysteresis. In particular, the two branches of the major hysteresis loop are not complementary to each other.

III. NUMERICS

As mentioned earlier, the pillars are modeled as single degrees of freedom which follow the LLG equation of motion. The effective field for each magnetic moment in the LLG equation is the "spin" derivative of the Hamiltonian of the previous section. Pillars are placed on a two-dimensional triangular lattice, to maximize the frustration of the dipolar bonds. All systems studied are 4×4 lattices with open boundary conditions. Unlike simulations of conventional condensed matter systems with $O(10^{23})$ particles, the array size chosen here is not an approximation because arrays could be fabricated with an arbitrary number of pillars. The size and boundary condition dependence of the phenomena we observe may have interesting features; this is left for future work. The positions of the pillars are $i\hat{\mathbf{x}} + j(\hat{\mathbf{x}}/2 + \hat{\mathbf{y}}\sqrt{3}/2)$ with $i,j = 0, \ldots, 3$. The orientation of the crystallographic axes is separately and randomly chosen for each pillar. Depending on the choice of these random orientations, a sample can have multicycles of various orders m, or a simple hysteresis loop (i.e., $m=1$). Square lattices are also considered.

The dimensions of the cylinders and the separation between them, the external field range, and the damping coefficient γ_2 are input parameters. These are used to calculate d_z, K_1, K_2, and the elements of $\mathsf{A}(\mathbf{r}_{ij})$. All the input parameters can be adjusted to maximize the occurrence of multicycles, except γ_2. Since γ_2 is a property of the material, but is unknown, we make sure that the results reported here are valid over a wide range of γ_2: essentially the entire $(0,\infty)$ range for multicycles, and $0.0005 < \gamma_2 < 50$ for asymmetric major hysteresis loops, which should include the experimentally appropriate value. For instance, in NiFe films, γ_2/γ_1 is measured to be 0.013 [17]. As long as the ratio γ_2/γ_1 is finite, the major hysteresis loop will be asymmetric, although the asymmetry will become small as $\gamma_2 \to \infty$ and the dynamics are effectively Ising-like.

Numerical modeling of the adiabatic field variation is straightforward. The external field is lowered or raised by a small field step δB_e. To optimize speed, the field step δB_e is adjusted adaptively, since a small step is required during avalanches. The effective field is then calculated and the system evolves by a small time step δt with this field. This time evolution is repeated, without changing B_e. Numerical integration of the LLG equation is implemented using the fourth-order Runge-Kutta algorithm. Once the system "settles" to a stationary state, the external field is changed again. Waiting for the system to reach a stationary state is equivalent to varying B_e more slowly than all the dynamics of the system, i.e., adiabatically. The time scale of an avalanche is presumed to be very short; therefore during an avalanche, δB_e is adjusted to be extremely small to maintain adiabatic change.

The requirement for settling is that the configuration after the evolution by a time step δt is essentially the same as the configuration before. In practice, some numerical tolerance is allowed, and the initial and final configurations must differ by less than this tolerance. The sums $\delta s_{x,i}^2 + \delta s_{y,i}^2 + \delta s_{z,i}^2$ for each i and $\Sigma_i \delta s_{z,i}$ must all be less than 10^{-11} in one time step for the system to be considered stationary. The results reported here are insensitive to a reduction of δB_e, δt, or the tolerance, and therefore represent adiabatic field variation with continuous time dynamics.

Starting from a large positive B_e (so that all the pillars are magnetized upward) the external field is lowered and cycled adiabatically over a range $[-B_e^{max}, B_e^{max}]$. The configuration $\{\mathbf{s}_i\}$ is compared at B_e^{max} after each cycle. If $\{\mathbf{s}_i\}$ is the same after every m occurrences of $B_e = B_e^{max}$, the system is in an m-cycle. Similar to the condition for settling, the configurations match up to a tolerance; we have verified in numerous cases that the tolerance does not introduce spurious multicycles. A tolerance of 10^{-4} for each component of the magnetization was found to be sufficient. Initially, the system undergoes a transient period of a few cycles of B_e before reaching a limit cycle.

Figure 1 shows the major hysteresis loop for a sample realization of randomness. Since all the pillars are magnetized vertically each time $B_e = \pm B_e^{max} = \pm\infty$, m is trivially equal to 1. However, one can see the avalanching dynamics characteristic of this system, and the fact—discussed earlier—that the ascending and descending branches of the major loop are not complementary. Figure 2 shows a hysteresis minor loop with a two-cycle.

IV. RESULTS

Using an algorithm that performs the operations of the previous section, we search through a large number of real-

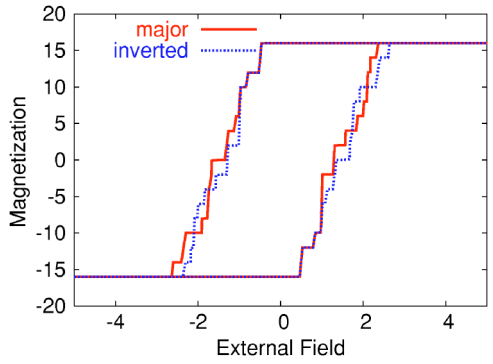

FIG. 1. Major hysteresis loop (solid curve) for a 4×4 triangular lattice of pillars. The steps demonstrate avalanching dynamics. In order to see that the ascending and descending branches of the loop are not complementary, the dashed curve shows the same hysteresis loop, with $\mathbf{M}\rightarrow-\mathbf{M}$ and $\mathbf{B}\rightarrow-\mathbf{B}$; the solid and dashed curves clearly do not coincide.

izations of randomness to find regions in parameter space where the probability of finding multicycles is high. The parameters in the model are the radius R and height h of the pillars, B_e^{max}, and the damping coefficient γ_2. If the lattice spacing, R, and h are all scaled by a factor λ, all the terms in the Hamiltonian are scaled by λ^3, which does not affect the ratios of the terms. Accordingly, the lattice spacing can be set to 100 nm without loss of generality. Given a set of parameters, the algorithm determines the periodicity m for a given realization of randomness. By classifying the periodicity for a large number of realizations, we obtained the approximate probability for finding an m-cycle as a function of m.

The easiest parameter to vary experimentally is B_e^{max}. As mentioned in the previous section, when B_e^{max} is too large or too small, multicycles will not be present. We find that multicycles can be roughly optimally found when B_e^{max} approaches the saturation field B_e^{sat} but not greater. B_e^{sat} is different for every realization of randomness; therefore the

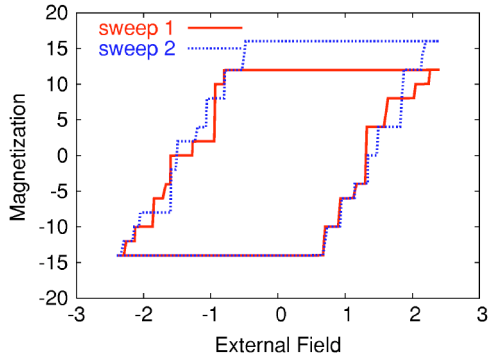

FIG. 2. A hysteresis two-cycle, starting at $B_e=-B_e^{max}$. The solid curve is a hysteresis loop after one cycle of the external field. The dashed curve is the hysteresis loop after the second cycle. Another sweep of the external field would retrace the solid curve, indicating that this particular realization of randomness undergoes a two-cycle. B_e^{max} is less than the saturation field B_e^{sat}. (If B_e^{max} were increased beyond B_e^{sat}, no multicycles would be found. Thus the two-cycle shown in this figure is a minor loop.)

TABLE II. Approximate probabilities of finding an m-cycle for systems with pillars of different radii. The lattice spacing is 100 nm and the aspect ratio h/R is 5.

R (nm)	$P_{m=2}$	$P_{m=3}$	$P_{m=4}$	$P_{m>4}$	$P_{m>1}$
10	0	0	0	0	0
20	0.08	0.02	0	0	0.1
25	0.14	0.12	0.02	0.04	0.32
30	0.2	0.06	0.04	0.16	0.46
35	0.22	0.22	0.04	0.12	0.6
40	0.22	0.12	0.1	0.18	0.62
45	0.28	0.12	0	0.10	0.50

optimal field can only be determined by scanning over various values of B_e^{max}. The range of B_e^{max} where the occurrence of multicycles is appreciable depends on the pillar dimensions. For $R=30$ nm and $h=180$ nm, the probability of finding multicycles when B_e^{max} is optimal is $\sim2-3$ times the probability when B_e^{max} is $\sim15\%$ smaller than the optimal field. In general, for systems in which the probability of finding multicycles is small, the range of B_e^{max} where the probability is nonzero is narrow. The narrow range in B_e^{max} is not an obstacle to finding multicycles due to the ease of tuning this parameter experimentally.

The damping coefficient of the LLG equation, γ_2, cannot be easily calculated. In fact, different experimental environments could allow for a large range of γ_2. Because of our inability to obtain a reasonable and realistic approximation for γ_2, we run searches for a wide range of γ_2 (relative to γ_1). The results show that multicycles exist for very small γ_2 to essentially infinite damping. (The large damping limit is implemented by setting $\gamma_1=0$ and keeping γ_2 finite.) Small values of γ_2 tend to give more multicycles, as one might expect: the probability of finding multicycles increases by a factor of ~1.5 when γ_2 is reduced from γ_1 to $\sim0.1\gamma_1$. Unexpectedly, the multicycle probability also seems to increase slightly when γ_2 is larger than γ_1. When the dynamical equation is strictly dissipative ($\gamma_1=0$), the multicycle probability is comparable to the probability when $\gamma_2\gtrsim\gamma_1$. There are no clear trends in the distribution of m when γ_2 is changed.

Because of the difficulty in calculating γ_2, we conservatively set γ_2 to a value where the probability of finding multicycles is approximately minimal. As mentioned in the preceding paragraph, this occurs when $\gamma_2\approx\gamma_1$. With B_e^{max} at its optimal value, and $\gamma_2=\gamma_1=1$, the probabilities of finding multicycles for systems with pillars of different R and h are found. The different terms in the Hamiltonian scale differently as R and h are varied. Table II shows results for systems of the same aspect ratio ($h/R=5$) and different radii. The pillar radius cannot be larger than ~45 nm with a lattice spacing of 100 nm. From Table II, one can see that systems of pillars with larger radii generally display multicycles more often.

The occurrence of multicycles depends largely on the aspect ratio of the pillars. Avalanches tend to occur only for pillars where h/R is large; accordingly, systems with disk-

TABLE III. Approximate probabilities of finding an m-cycle for systems with pillars of different aspect ratios h/R. The lattice spacing is 100 nm and the radius is fixed at 30 nm.

h/R	$P_{m=2}$	$P_{m=3}$	$P_{m=4}$	$P_{m>4}$	$P_{m>1}$
0.5	0	0	0	0	0
1	0	0	0	0	0
3	0.16	0.04	0.02	0.12	0.34
4	0.12	0.08	0.02	0.16	0.38
5	0.2	0.06	0.04	0.16	0.46
6	0.16	0.1	0.06	0.16	0.48
10	0.24	0.2	0.06	0.1	0.6

shaped pillars, i.e., with negative d_z, do not display multicycles. In fact, even when d_z is positive, multicycles are only found for a sufficiently large shape anisotropy energy. Table III shows numerical results for systems of pillars with a 30 nm radius and various aspect ratios. Multicycles are only likely to be found for systems with long pillars. No multicycles are found for disk-shaped pillars as expected.

Systems with pillar vacancies are also studied. Vacancies are implemented by introducing a finite probability for a pillar to be missing at every lattice site. One might expect that these vacancies would introduce more randomness in the system, thereby increasing the number of multicycles. For pillars with $R=30$ nm and $h=150$ nm, the probability of finding a multicycle is ~ 0.46 without any vacancies. When the probability of having a vacancy at a site is small (~ 0.2), the number of multicycles drops by about 40%. When the vacancy probability increases to $\gtrsim 0.5$, the probability of finding multicycles decreases to less than 0.1. This decrease in probability could be due to the decrease in the number of pillars. We conclude that, contrary to what one might expect, random vacancies do not increase the probability of multicycles.

The probability of finding a multicycle is significantly less on a square lattice than on a triangular lattice; for a pillar array arranged in a square lattice, the probability of finding a multicycle is approximately half of the corresponding probability for a triangular lattice. We speculate that this difference in probabilities could be due to the different amount of frustration between the configurations. If a square lattice is used instead of a triangular one, the dipolar couplings between nearest neighbor pillars are not frustrated. In a checkerboard pattern, all nearest neighbor bonds would be satisfied, but the next nearest neighbor bonds (and certain neighbors further apart) would not be satisfied. Thus, if frustration is important for the existence of multicycles, multicycles are expected to be much less probable on a square lattice.

A possible mechanism for increasing frustration and disorder is to introduce random ferromagnetic couplings between pillars. These bonds could be manufactured by building one large pillar instead of two small ones. The large pillar would have two domains that are coupled ferromagnetically. By randomly assigning the bonds with some probability, more disorder can be introduced in addition to that from the crystalline anisotropy. We did not study how these ferromagnetic bonds affect the number of multicycles.

One interesting question is whether exact return point memory [12] survives when it is extended beyond the random field Ising model with purely ferromagnetic interactions to continuous time vector models. To answer that, we use the LLG model with nearest neighbor random ferromagnetic interactions and the same crystalline and shape anisotropy model that is used above (without dipole coupling). We apply a random field and search for violations of RPM with different random seeds. We start at high fields and go to a minimum field of -1.7 and record the spin configuration. Then we go up to a field 1.7 and back down to -1.7. We find that for a 4×4 square lattice of spins, of the order of 1% of systems *violate* RPM because the initial and final minimum configurations and total magnetization are substantially different. Violation of RPM is seen both with and without the precessional term in Eq. (1). This shows that it is not possible to extend the proof of RPM to continuous vector models.

V. CONCLUSIONS

In this paper, we have investigated the feasibility of observing multicycles and noncomplementary hysteresis loops in a candidate experimental system: that of cylindrical magnetic nanopillars arranged on a lattice. We have performed realistic numerical simulations of this system by calculating the magnetic interactions between the pillars and then employing continuous spin dynamics and the Landau-Lifshitz-Gilbert equation to obtain their time evolution. Using physically appropriate parameters, we have shown that there is often multicycle hysteretic behavior, i.e., a periodic adiabatic external magnetic field causes a subharmonic steady state response in the magnetization. Because systems of this kind are currently the subject of much experimental investigation, we believe that it would be fruitful to attempt to observe the unusual behavior predicted here.

We have also shown that, even though the Hamiltonian is invariant under spin and external field reversal, the dynamics are not, so that the ascending and descending branches of the major hysteresis loop are not complementary. This result requires both a precessional and a relaxational term in the dynamics, emphasizing the importance of both. In particular, since it is impossible to include precession for Ising models, they are—despite their ubiquitousness for strongly anisotropic magnets—qualitatively inadequate in certain respects. Further implications of the noncomplementary nature of LLG dynamics will be studied elsewhere [14] and in future research.

ACKNOWLEDGMENTS

We thank John Donohue, Holger Schmidt, Mark Sherwin, and Larry Sorensen for very useful discussions.

[1] C. P. Steinmetz, Trans. Am. Inst. Electr. Eng. **9**, 3 (1892).
[2] H. Barkhausen, Z. Phys. **20**, 401 (1919).
[3] J. Katz, J. Phys. Colloid Chem. **53**, 1166 (1949); P. H. Emmett and M. Cines, *ibid.* **51**, 1248 (1947).
[4] Z. Z. Wang and N. P. Ong, Phys. Rev. B **34**, 5967 (1986).
[5] J. Ortin and L. Delaey, Int. J. Non-Linear Mech. **37**, 1275 (2002), and references therein; J. Ortin, J. Appl. Phys. **71**, 1454 (1992).
[6] *Magnetic Recording Technology*, 2nd ed., edited by C. D. Mee and E. D. Daniel (McGraw-Hill Professional, New York, 1996).
[7] J. M. Deutsch and O. Narayan, Phys. Rev. Lett. **91**, 200601 (2003).
[8] K. H. Fischer and J. A. Hertz, *Spin Glasses* (Cambridge University Press, Cambridge, U.K., 1991), and references therein.
[9] M. C. Abraham, H. Schmidt, T. A. Savas, H. I. Smith, C. A. Rose, and R. J. Ram, J. Appl. Phys. **89**, 5661 (2001); H. Schmidt and R. J. Ram, *ibid.* **89**, 507 (2001).
[10] S. H. Charap, P. L. Lu, and Y. He, IEEE Trans. Magn. **33**, 978 (1997); H. N. Bertram, H. Zhou, and R. Gustafson, *ibid.* **34**, 1845 (1998); D. Weller and A. Moser, *ibid.* **35**, 4423 (1999).
[11] S. Sabhapandit, D. Dhar, and P. Shukla, Phys. Rev. Lett. **88**, 197202 (2002).
[12] J. P. Sethna, K. Dahmen, S. Kartha, J. A. Krumhansl, B. W. Roberts, and J. D. Shore, Phys. Rev. Lett. **70**, 3347 (1993).
[13] J. A. Barker, D. E. Schreiber, B. G. Huth, and D. H. Everett, Proc. R. Soc. London, Ser. A **386**, 251 (1983); J. Ortin, J. Appl. Phys. **71**, 1454 (1992).
[14] M. S. Pierce *et al.*, Phys. Rev. Lett. **90**, 175502 (2003); **94** 017202 (2005).
[15] F. H. de Leeuw, R. van den Doel, and U. Enz, Rep. Prog. Phys. **43**, 689 (1980).
[16] E. C. Stoner and E. P. Wohlfarth, Philos. Trans. R. Soc. London, Ser. A **240**, 599 (1948).
[17] G. M. Sandler *et al.*, J. Appl. Phys. **85**, 5080 (1999).